DOI 10.1007/s12541-009-0046-8

Sliding Mode Control of the Inchworm Displacement with Hysteresis Compensation

Insoo Kim[1,#], Yeung-Shik Kim[1] and Eun-Cheol Park[2]

1 Department of Mechanical Engineering, Kumoh National Institute of Technology, 1, Yangho-dong, Gumi, Gyeongbuk, South Korea, 730-701
2 Hanwha Co., Ltd., 258, Gongdan-dong, Gumi, Gyeongbuk, South Korea, 730-904
Corresponding Author / E-mail: kiminsoo@kumoh.ac.kr, TEL: +82-54-478-7345, FAX: +82-54-478-7319

KEYWORDS: Inchworm, Hysteresis, Sliding mode control, Kalman filter, Residual vibration, System identification in frequency domain

This paper proposes a new modeling scheme to describe the hysteresis and the preload characteristics of piezoelectric stack actuators in the inchworm. From the analysis of piezoelectric stack actuator behavior, the hysteresis can be described by the functions of a maximum input voltage and the preload. The dynamic characteristics are also identified by the frequency domain modeling technique based on the experimental data. The hysteresis is compensated by the inverse hysteresis model for precise control of inchworm displacement. Since the dynamic stiffness of an inchworm is generally low compared to its driving condition, the mechanical vibration may degrade accuracy of the inchworm. Therefore, the SMC (Sliding Mode Control) and the Kalman filter are developed for the motion control of the inchworm. The feasibility of the proposed modeling scheme and the control algorithm is tested and verified experimentally.

Manuscript received: March 19, 2008 / Accepted: March 3, 2009

NOMENCLATURE

V_{in} = input voltage of piezoelectric actuator
X_r, X_f = displacements of piezoelectric actuator for extension and shrinkage.
$u(k)$ = output of sliding mode controller
S_n = signum function
β = model uncertainty
L = gain of Kalman filter

1. Introduction

The need of the high precision driving equipment[1] is being dramatically increased in the field of semiconductor, LCD equipments, machine tools, cell biology and measurement technology etc.. Recently many researches on the piezoelectric materials have been performed. the piezoelectric materials may be used for not only various actuators but also various sensors. The piezoelectric materials have the good properties for actuator and sensor such as light and small size, high speed response, high power and resolution.[2] Various actuator using piezoelectric materials are being continually developed,[3-6] i.e., a linear device moving along the friction surface using impact drive mechanism, an inch-worm type that produces large displacement through the repetition of extension and shrinkage among three piezoelectric actuators, a tube type piezoelectric actuator which is used in scanner device equipment for high precision surface measurement and a slider using friction force generated by two stack type piezoelectric actuators etc..

Since the piezoelectric element has highly nonlinear characteristics, it degrades the accuracy of the system. To incorporate these nonlinearities in the modeling process, many researches have been performed. Kaizuka et al. removed nonlinearities by connecting capacitor in series between input voltage amplifier and piezoelectric actuator.[7] However, it needs relatively high voltage in operation. Goldfarb et al.[8] described the hysteresis characteristic using Maxwell model. Ge et al. modeled the hysteresis characteristic using Preisach model.[9] However, this model is available for only a constant, repetitive, and periodic signal. Tzen et al.[10] proposed a numerical expression by approaching geometric shape of the hysteresis to the exponential function. The dynamic stiffness of inchworm during motion

operation is generally low compared to its driving condition, so that mechanical vibration of inchworm degrades accuracy of the displacement. Therefore, a robust control algorithm[11-14] to suppress the mechanical vibration of a system are required.

The purpose of this paper is to develop a new modeling scheme to incorporate the nonlinearities of the piezoelectric stack actuator and the preload characteristics of the inchworm. For the precision motion control, the hysteresis behavior is compensated by the inverse hysteresis model and the sliding mode control and the Kalman filter are developed to suppress the mechanical vibration of inchworm. Experiment is performed to show the feasibility of the proposed modeling scheme and control algorithm.

2. Modeling of the Inchworm

2.1 Specifications of Inchworm

An inchworm which is a linear moving device is developed to produce a large displacement from the transformation of stack piezoelectric actuators. Even though the transformation quantity of piezoelectric actuators is just several micrometers, the inchworm generates large displacement along the moving guide surfaces using a friction mechanism as a worm crawls. Fig. 1 describes one cycle of inchworm motion which is composed of six processes. To find the dynamic characteristic of piezoelectric actuator, the frame including the propulsion part of the inchworm is mounted at the

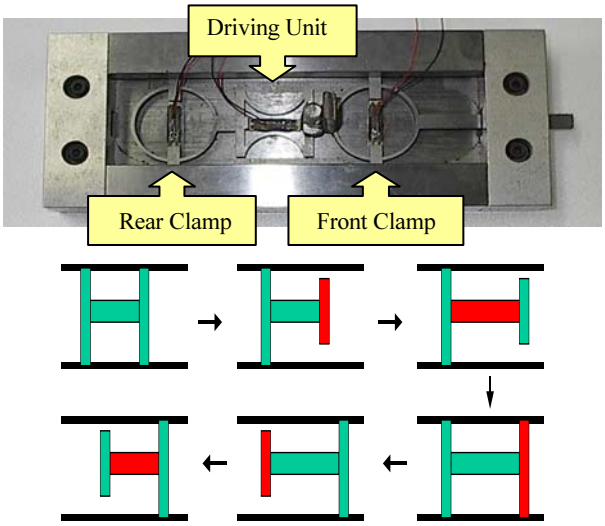

Fig. 1 The structure and the operation diagram of the inchworm

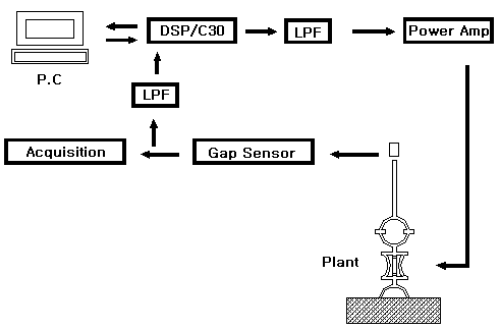

Fig. 2 The experiment device for propulsion part of inchworm

experiment device shown in Fig. 2. The piezoelectric actuator is 21mm length and has 150 piezoelectric thin layers. Table 1 shows its specification. In experimental modeling process, signal generator (LMS, CADA-X with Scadas II front-end), FFT analyzer (LMS, DI-2200), and digital signal processor (Loughborough, TMS320C40) are used for the hysteresis modeling and the frequency domain identification.

Table 1 The Specification of piezoelectric stack actuator

MODEL	15C	Unit
Capacitance	900±20%	C(nF)
Insulation Resistance	$>1\times10^8$	Ro(Ω)
Max. Driving Field	150	Eo(V)
Effective Displacement	20±2	Xo(μm)
Xo/Eo	0.16	(μm/V)
Material	SPEM-5D	
Response Time	20μsec	
Maximum Clamping Force	700	N

2.2 Hysteresis Modeling without Preload

The behavior of the inchworm consists of both the hysteretic nonlinearity and the dynamic characteristics. To describe the hysteresis of an actuator, a linearly decreasing triangle wave of low frequency input signal is applied to the actuator to eliminate the effects of dynamic characteristics. From the hysteresis loops shown in Fig. 3, following properties are assumed. First, the hysteresis loops are divided into an initial rising curve, repetitive falling (shrinkage) curves and repetitive rising (extension) curves. Second, the shape of the hysteresis loops is changed by V_{max} (maximum input voltages). Third, the residual displacement exists when input voltage is removed as indicated in Fig. 3 and is also changed by V_{max}. The discrepancy between the initial value of the initial rising curve and the lowest value of other curves is caused by microscopic ferroelectric polarization effect of PZT stack. Only the plus voltage is applied to PZT stack as shown in Fig. 3. Size of hysteresis loop is increased as the range of applied voltage is increased. From the analysis of hysteresis loops behaviors, each curve can be described by the second-order polynomial function of argument V_{in} (input voltage) and the coefficients of the polynomial are to be determined. The hysteresis loops are now described by the following equations

$$X_r = D_r + C_{r1} \times V_{in} + C_{r2} \times V_{in}^2 \tag{1}$$

$$X_f = D_f + C_{f1} \times V_{in} + C_{f2} \times V_{in}^2 \tag{2}$$

where V_{in} is an input voltage. The subscripts of r and f in the equations indicate the rising and the falling curves, respectively. X_r and X_f are output displacements, D_r and D_f are residual displacements, and C_{r1} and C_{r2} are coefficients for rising curves and C_{f1} and C_{f2} are coefficient for falling curves. In order to determine these coefficients in Equations (1) and (2), the hysteresis loops are analyzed with the change of various input voltages. It is observed that the shape and the residual displacement of hysteresis loops are varied by the magnitude of applied V_{max}.

To figure out the behavior of hysteresis loops against V_p (transition peak point voltage), the triangle input voltage of 2Hz is

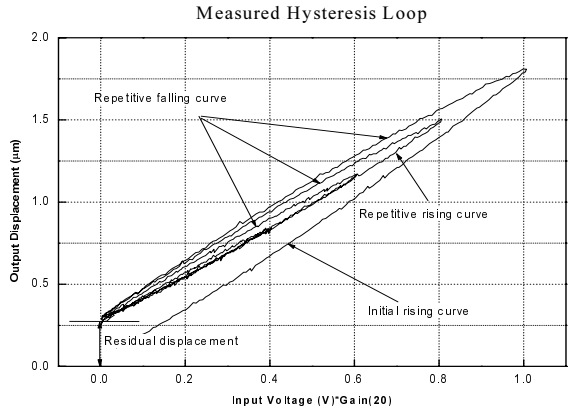

Fig. 3 Hysteresis loop for decreasing input sine wave

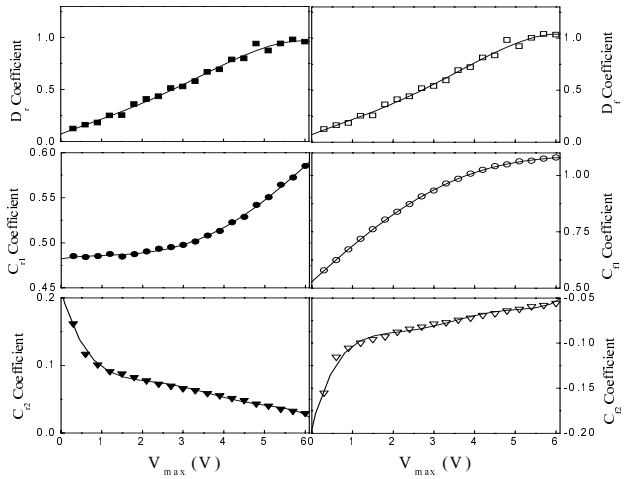

Fig. 4 The identified coefficients by curve fitting

applied to the actuator starting from 6 volt to 120 volt increasing by 6volt. Each hysteresis loop is modeled by the curve fitting method determining all coefficients, D_r, D_f, C_{r1}, C_{r2}, C_{f1}, C_{f2}. Fig. 4 shows all coefficient values. From this figure, it is observed that each coefficient is a function of V_{max} and each curve is described by the second-order polynomial function of argument V_{max}. From the analysis of hysteresis loop behaviors, each curve is described by the second-order polynomial function of argument V_{in} and the coefficients of the polynomial are described by the function of argument V_{max}.

Followings are the procedures for determining the coefficients in Equation (1) and (2) and the flowchart is shown in Fig. 5. Simulation starts when first input voltage is applied to the system. The coefficients of initial rising function, D_r, C_{r1}, C_{r2}, substitute into Equation (1). The coefficients of initial rising function are fixed until the direction of the input voltage changed.

When the input voltage reaches peak point, decide whether the direction of input voltage is down or up. Then determine the output displacement by Equations (1) and (2). If the input voltage reaches first peak, the maximum input voltage is updated by new V_{max}. Then the coefficients of function $X_f(V_{in})$ are updated and fixed until new V_{max} reaches. Fig. 6 shows the comparisons of the hysteresis loops and the modeling error between measured and simulated data is within 0.125μm.

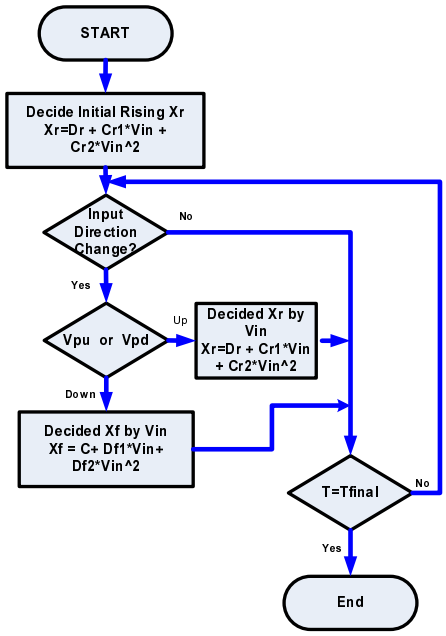

Fig. 5 Flow chart for hysteresis loop modeling

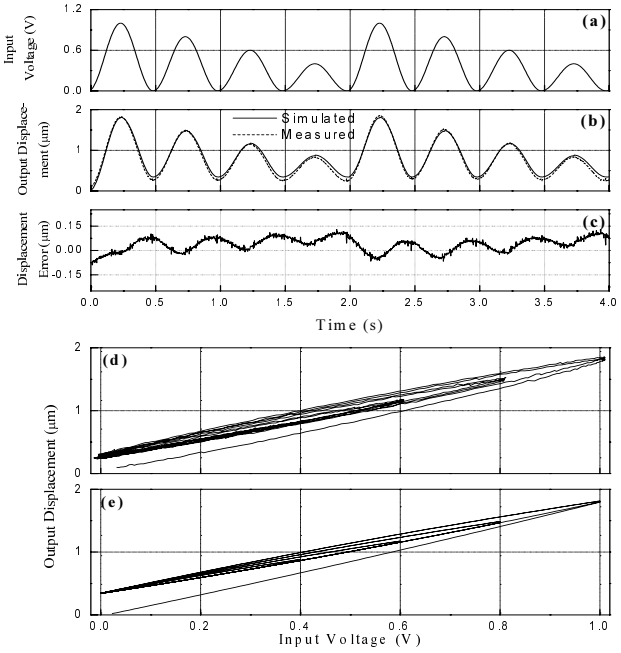

Fig. 6 Simulated and measured data; (a) input voltage, (b) measured displacement (dashed) and simulated displacement (solid), (c) modeling error, (d) measured hysteresis loop, (e) simulated hysteresis loop

2.3 Hysteresis Modeling under Preload

Inchworm in this paper is designed for high precision positioning device with low constant payload (or no payload), low energy consumption for operation and large translational movement per cycle. Because the preload is not used to prevent hysteresis of a PZT stack in this research, only a low preload (5N) is applied to the PZT stack. Note that when preload is increased, hysteresis of a PZT stack is reduced and the necessary energy to extend the PZT stack (or to operate inchworm) is also increased and deformation range of propulsion part of inchworm is decreased.

In the modeling process, the preload applied to the inchworm must be considered. Fig. 7 shows the schematic of the experiment to study how the preload affects the displacement of the inchworm. The effect of a piezoelectric actuator to the preload variations is examined. Fig. 8(a) shows the changes of output displacement to the variation of preload varying input voltages. As the results of the experiment, we observed that the preload up to 6N does not affect much the output displacement of the piezoelectric actuator since the maximum clamping force of the piezoelectric element is 700N as shown in Table 1. Fig. 8(b) shows the variations of the hysteresis loops to the preload with 60V input sine wave. There are no serious changes of hysteresis loops. However, the preload seriously affects the inchworm because the frame of front fixed part as shown in Fig. 1 makes a role of mechanical spring. Fig. 9 shows compressed displacements at the tip of the inchworm varying the preload. From Fig. 9, we observed that the displacement at the tip of the inchworm varies linear to the applied preload and the mechanical propulsion part of inchworm is designed to be very flexible structurally (stiffness: 0.41N/μm).

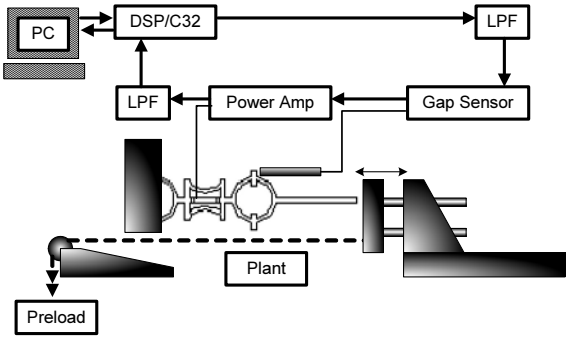

Fig. 7 The experimental setup for preload characteristic

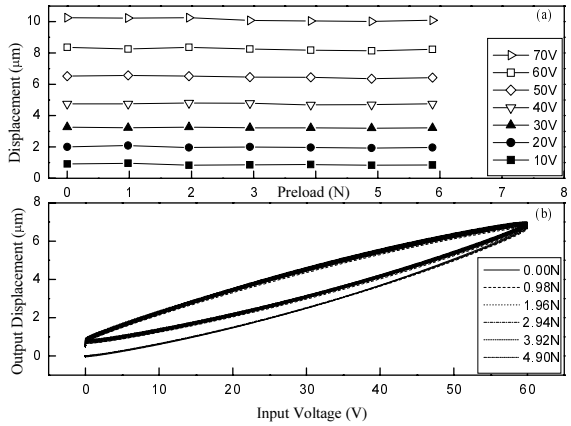

Fig. 8 (a) Preload vs. displacement varying input voltage, (b) hysteresis loop with preload

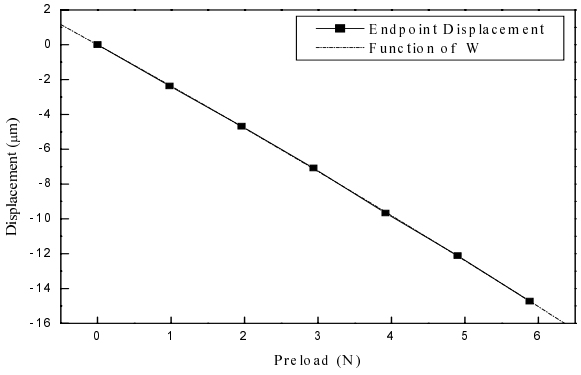

Fig. 9 The compressed displacement of inchworm by preload

To incorporate the preload effect in the modeling process, the following equation is suggested as

$$W = A_1 + B_1 \times L_o + B_2 \times L_o^{\,2} \tag{3}$$

Where L_o is magnitude of preload, A_1, B_1, and B_2 are coefficients, W is the compressed displacement of the inchworm by preload. The equation (3) is added into Equations (1) and (2) and rewritten as

To incorporate the preload effect in the modeling process, the following equation is suggested as

$$X_r = D_r + C_{r1} \times V_{in} + C_{r2} \times V_{in}^2 + W \tag{4}$$

$$X_f = D_f + C_{f1} \times V_{in} + C_{f2} \times V_{in}^2 + W \tag{5}$$

Fig. 10 shows the hysteresis loops of the experimentally measured and the calculated displacement using identified model of inchworm in case of applying 5.88N preload and 20V input sine wave. This figure shows a good agreement between calculated and measured displacements.

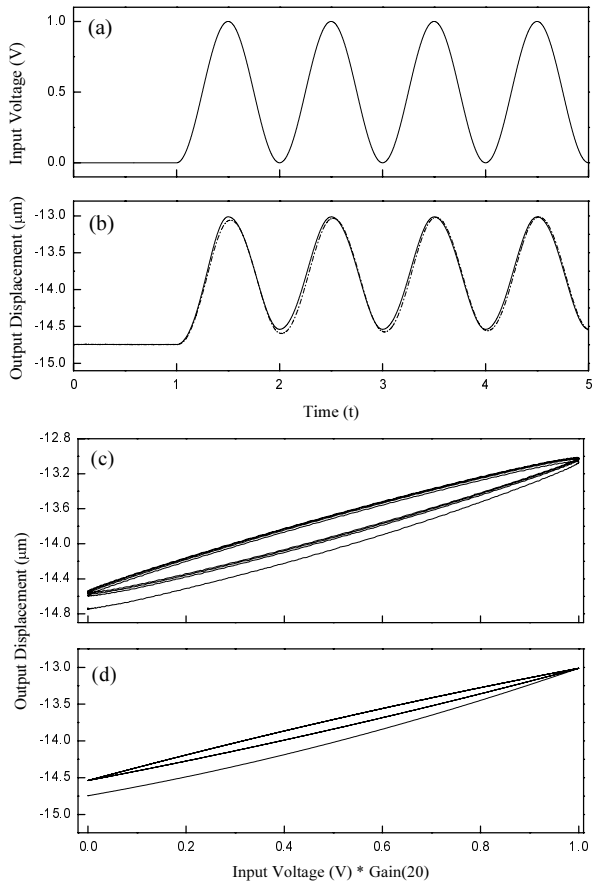

Fig. 10 Calculated and measured data with 5.88N preload; (a) input voltage, (b) measured displacement (dashed) and calculated displacement (solid), (c) measured hysteresis loop, (d) calculated hysteresis loop

2.4 Modeling of Dynamic Characteristics

Dynamic characteristic of inchworm is remained constant because the inchworm is operated under no payload (or a low constant payload). And control strategy is not considering of the time variant system or payload. The experimental identification process is used to model the dynamic characteristics of inchworm because theoretical modeling for inchworm shows the some practical limit. In this study, among many frequency domain identification methods, the novel method using the matrix-fraction rather rational matrix function for the curve fitting is adopted.[15] This method enables curve-fitting operation to be linear and requires no iteration calculation. The frequency domain identification procedure is performed by the following procedure. First, acquire frequency responses from input and output data sequences. Second, curve-fit the frequency response function using the matrix fraction description method. Third, conduct minimum realization, which cancels matched poles and zeros within a tolerance.

Fig. 11 shows comparison between the measured and modeled frequency responses. Modeling order of the system is determined as 3. Interest bandwidth is 1 kHz at the center of 635Hz.

Fig. 12 shows a reference square input and the measured output of uncontrolled inchworm system. Although the system operates under low frequency, it shows the dynamic characteristic due to square input. The reference input voltage of each step is 1V and period of each step is 0.4sec. It is shown that the system has dynamic characteristic of the system together with the hysteresis of the piezoelectric actuator. The maximum overshoot is 3.8㎛ and the residual vibration still remains after a half of period.

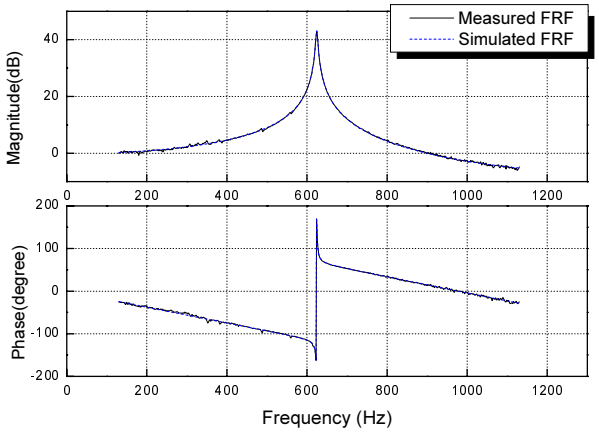

Fig. 11 Frequency response function

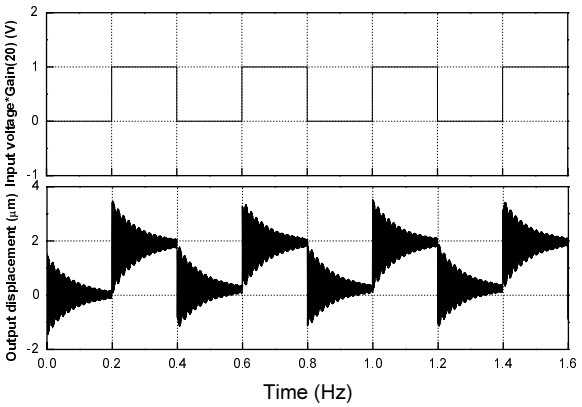

Fig. 12 Input and uncontrolled output displacement

3. Controller Design

3.1 Sliding Mode Controller (SMC)

Consider the nth order linear time invariant system with m inputs and known uncertainty f which can be obtained by the experimental identification process given by

$$x(k+1) = Ax(k) + Bu(k) + f(k,x,u) \tag{6}$$

$$f(k,x,u) = B\xi(k,x,u) \tag{7}$$

where A, B are system matrices or vectors related with system states $x(k)$, $u(k)$ is the control input and ξ presents uncertainties or nonlinearities. Define a switching function s(k) as

$$s(k) = Sx(k) \tag{8}$$

where $S \in R^{m\times n}$ is of full rank and the hyperplane is defined as $S = \{x \in R^n : s(x) = 0\}$ and is designed from reference.[13] SMC $u(k)$ has two part, linear feedback component (u_l) and nonlinear feedback component (u_n). The SMC law can be expressed as

$$u(k) = u_l(k) + u_n(k) \tag{9}$$

where

$$u_l(k) = -\wedge^{-1}(SB - \Phi S)x(k) \tag{10}$$

$$u_n(k) = -(\eta\|\Lambda\|^{-1}\|s(k)\| + \beta)S_n(s(k)) \tag{11}$$

$$S_n(s(k)) = \frac{s(k)}{|s(k)| + \delta} \tag{12}$$

where $\Lambda = SB$. η is positive scalar. β is model uncertainty, and Φ is eigenvalue of the switching function which makes chattering amplitude lower and reaching time to the sliding surface faster. $S_n(s(k))$ is a signum function and the slop of the signum function depends on δ.

3.2 Observer Design

In practice, not all state variables are available from direct measurement. In order to form the desired control output it is necessary to estimate the state variables that are not directly measurable. Current type Kalman filter may be used to estimate all state variables based on the measured output:

$$\hat{x}(k+1) = A\hat{x}(k) + Bu(k) + L(y(k) - C\hat{x}(k) - Du(k)) \tag{13}$$

where $\hat{x}(k)$ and L are the estimated state variables and gain of Kalman filter respectively. y is a measured displacement. Gain of current type Kalman filter is determined by the following equation that minimizes covariance of error $(x(k) - \hat{x}(k))$.

$$L = APC^T(R_0 + CPC^T)^{-1} \tag{14}$$

where P is a solution of Riccati equation expressed as

$$P = APA^T - APC^T(R_0 + CPC^T)^{-1}CPA^T + LQ_0L^T \qquad (15)$$

where R_0 and Q_0 are gain matrices.

4. Experimental Result

4.1 Open-loop Control using Hysteresis Modeling

The modeling method of the hysteretic characteristics was described in section 2. The inverse hysteresis model is needed for the control implementation. It can be achieved by removing hysteretic characteristics of the system so that the relationship between inputs and outputs is linear. The procedures for the inverse hysteresis modeling are following. First, multiply the output displacement by constant rate, second, compensate the difference between input voltage and output displacement, and finally obtain the compensated input voltage. The procedure is described by the following equation

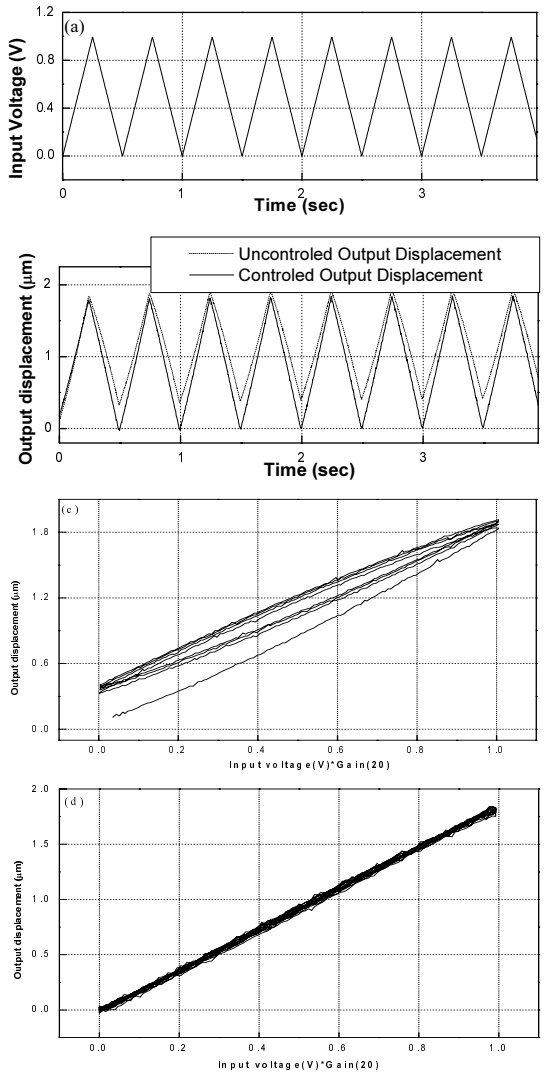

Fig. 13 Eperimental results of open loop control to regular triangle signal; (a) input voltage (b) measured output displacements of uncontrolled and controlled systems (c) measured hysteresis loop of uncontrolled system (d) measured hysteresis loop of controlled system

$$\begin{aligned} u_{com}(k) &= V_r(k) - X_r(k) \times R \\ u_{com}(k) &= V_r(k) - X_f(k) \times R \end{aligned} \qquad (16)$$

where R is a rate, $V_r(k)$ is the reference input voltage, $X_r(k)$ and $X_f(k)$ are the displacements derived from Equations (1) and (2), and $u_{com}(k)$ is the compensated input voltage.

Fig. 13 shows the relationship between an input voltage and output displacements with an open-loop control. In the modeling process, set the value of the rate be 0.5475. The reference input is the triangle wave of 2Hz shown in Fig. 13(a). Fig. 13(b) shows the comparison of output displacements with compensation (solid line) and without compensation (dot line). Fig. 13(c) and (d) show the hysteresis loops without compensation and with compensation, respectively. The inverse hysteresis modeling is performed well as shown in this figures.

4.2 SMC based on the Dynamic Characteristics Modeling

The sliding mode control is applied to suppress the mechanical vibration of the inchworm. The hysteresis of the actuator is not considered in the dynamic model. The block diagram of the control system is shown as Fig. 14. The state matrix A and the input matrix B are derived from in section 2.4 and substituted into Equation (6). The transformation function S in Equation (8) is set at [-1.0744, -0.0904, 0.0781]. The gain of linear control term is set [0.5130, -1.6069, 1.1001]. Coefficients in the nonlinear control term are set η =0.002 and β =0.0002. Next, observer gain L in Equation (13) is set [0.0040, 0.5771, 0.3558]. Fig. 15 shows that the settling time is reduced from 0.5 to 0.02 and maximum overshoot is suppressed from 3.7㎛ to 2.25㎛. However, the system output doesn't become 0 ㎛ even though the reference input is 0 volt. This is due to the hysteretic characteristics of the system.

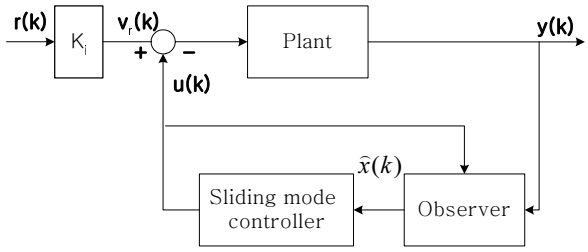

Fig. 14 Schematic of the servo control system

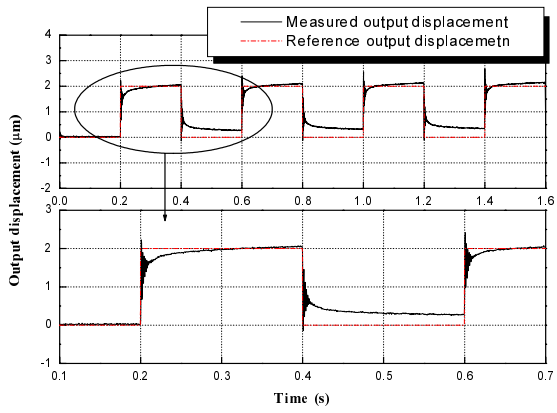

Fig. 15 Response of the system with sliding mode control

4.3 SMC based on the Hysteresis and Dynamic Characteristics Modeling

From Fig. 15, it is recognized that the hysteresis characteristic of a piezoelectric actuator must be considered. Both the hysteretic characteristics of the piezoelectric actuator and the dynamic characteristics of the inchworm are considered in the control process. Fig. 16 shows the block diagram of the control system. All values on SMC are same as the values in section 4.2.

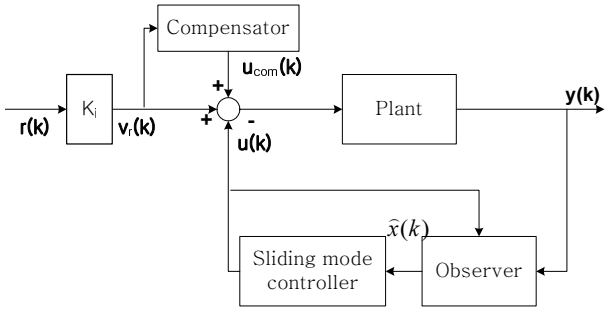

Fig. 16 Schematic diagram of the servo control with compensator

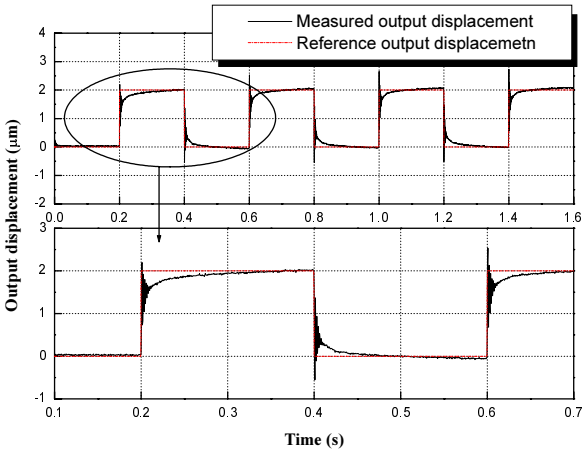

Fig. 17 Response of the controlled system with compensator

Fig. 17 shows the displacement of the controlled system. There exists the residual displacement of approximately 0.25㎛ in Fig. 15. But in Fig. 17, the residual displacement is removed by applying the compensator.

5. Conclusions

A modeling method for the hysteresis of piezoelectric actuator is presented. This model describes displacements of piezoelectric actuator for extension and shrinkage in a second-order polynomial function of input voltage and preload. Dynamic characteristic of the inchworm for control purpose is modeled experimentally using matrix-fraction curve fitting method in frequency domain.

The displacement of inchworm is controlled using sliding mode controller with Kalman filter designed on the base of identified model. Experimental result shows that the presented control scheme is effective for the displacement control of inchworm. The overshoot of output displacement is suppressed from 1.5㎛ to 0.2㎛, and the residual displacement of 0.25㎛ due to the hysteresis is completely removed.

REFERENCES

1. Choi, D. K., "Developing trend of automation elements for precise control," International Journal of Control, Automation and Systems, Vol. 6, Issue 1, pp. 33-38, 2000.
2. Slocum, A., "Precision Machine Design," Prentice-Hall, pp. 666-674, 1992.
3. Higuchi, T., Watanade, M. and Kudoh, K., "Precise Positioner Utilizing Rapid Deformations of a Piezoelectric Element," J. of Japan Society of Precision Engineering, Vol. 54, No. 11, pp. 2107-2112, 1988.
4. Kim, J. H. and Kim, J., "A Hybrid Inchworm Linear Motor," Mechatronics, Vol. 23, Issue 3, pp. 525-542, 2002.
5. Jung, H., "Hysteresis and Creep analysis of PZT Actuators and application," Ph.D. Thesis, KAIST, 2000.
6. Kim, S. C. and Kim, S. H., "A Precision Linear Actuator Using Piezoelectrically Driven Friction Force," Mechatronics, Vol. 11, Issue 8, pp. 969-985, 2001.
7. Kaizuka, H. and Siu, B., "A Simple Way to Reduce Hysteresis and Creep When Using Piezoelectric Actuators," Japanese Journal of Applied Physics, Vol. 27, No. 5, pp. L773-L776, 1988.
8. Goldfarb, M. and Celanvovic, N., "A Lumped Parameter Electromechanical Model for Describing the Nonlinear Behavior of Piezoelectric Actuators," ASME J. of Mechanical Design, Vol. 119, No. 3, pp. 478-485, 1997.
9. Ge, P. and Jouaneh, M., "Modeling Hysteresis in Piezoceramic Actuators," Precision Engineering, Vol. 17, No. 3, pp. 211-221, 1995.
10. Tzen, J., Jeng, S. and Chieng, W., "Modeling of Piezoelectric Actuator for Compensation and Controller Design," Precision Engineering, Vol. 27, No. 1, pp. 70-86, 2003.
11. Green, M. and Limebeer, D., "Linear Robust Control," Prentice Hall, pp. 215-262, 1995.
12. Yoon, J. H., Kim, Y. S. and Kim, I. S., "Motion Control of Inchworm," J. of KSPE, Vol. 19, No. 9, pp. 179-185, 2002.
13. Edward, C. and Spurgeon, S. K., "Sliding Mode Control, Theory and applications," Taylor and Francis Ltd, pp. 31-63, 1998.
14. Henmi, N. and Tanaka, M., "An Open-Loop Method for Point-to-Point Positioning of a Piezoelectric Actuator," International Journal of Precision Engineering and Manufacturing, Vol. 8, No. 2, pp. 9-13, 2007.
15. Juang, J. N., "Applied System Identification," Prentice Hall, pp. 229-254, 1994.